atmosphere

Article

Impacts of Urban Expansion on Relatively Smaller Surrounding Cities during Heat Waves

Bei Huang [1], Guang-heng Ni [1,*] and C. S. B. Grimmond [2]

1 Department of Hydraulic Engineering, Tsinghua University, Beijing 100084, China
2 Department of Meteorology, University of Reading, Reading RG6 6BB, UK
* Correspondence: ghni@tsinghua.edu.cn

Received: 28 May 2019; Accepted: 24 June 2019; Published: 1 July 2019

Abstract: Urban-induced thermal stress can threaten human health, especially during heat waves (HWs). The growth of cities further exacerbates this effect. Here, weather research and forecasting (WRF) with an urban canopy model (UCM) is used to assess the effects of megacities and their growth on the thermal regime of proximal cities during heat waves. Analysis of the heat fluxes shows that advection impacts cities downwind. Results indicate that as urban areas change size (50%–100% and 100–150% of their current size), the local 2 m temperature increases by 2.7 and 1.7 °C, and the 2 m specific humidity decreases by 2.1 and 1.4 g kg^{-1}, respectively. A small city downwind is impacted with a 0.3–0.4 °C increase in 2 m temperature. Green roof is a potential mitigation strategy for these regions (i.e., beyond the megacity). With 50% green roofs in an urban area, a 0.5 °C decrease in 2 m temperature and 0.6 g kg^{-1} increase in specific humidity is simulated. Urbanization upwind of a megacity will contribute to regional climate change.

Keywords: heatwave; urban expansion; city position; city size; green roofs

1. Introduction

Heat waves (HWs), excessively hot periods that last for several days or longer, are a key cause of weather-related mortality [1,2]. Urban citizens are more vulnerable to HWs, given the additional warmth in cities relative to rural surroundings, and the greater exposure of people to these conditions given greater population densities. During heat waves, greater heat-related deaths are predicted—for example, 148 deaths in Atlanta under a +2 °C scenario [3], or 700 documented in Chicago during a 1995 heat wave [4]. Epidemiological studies suggest the mortality risk increases by 3.74% during a heat wave compared to non-heat wave periods [1].

Land cover changes and land use-related waste heat emissions have significant impacts on the climate at local and regional scales by modifying the energy, water, and momentum exchanges between the surface and atmosphere. These exchanges influence air temperature, moisture, wind, and precipitation, resulting in distinct urban climates, including the well-known urban heat island (UHI) effect [5,6]. Recent theoretical, numerical, and experimental studies suggest that these urban effects may be enhanced during heat waves. Moreover, Li and Bou-Zeid [7] suggest that not only do heat waves increase the ambient temperatures, but they also intensify the difference between urban and rural temperatures. As a result, the added heat stress in cities is even higher than the sum of the background urban heat island effect and the heat wave effect. This means cities are even more vulnerable to HWs than other environments. A number of past studies have documented such urban effects. For example, a high-resolution (1 km) simulation of HW events concluded that the daily mean UHI in New York city increased the temperature by 1.5 °C [8]. Analysis of Beijing flux observations found that changes in the surface energy balance under HWs are responsible for the intensification of UHIs under HWs [9,10], with the role of wind speed being important but varying between cities [11].

The effects of urbanization on temperature and precipitation extend to surrounding rural areas and nearby downwind cities [12,13]. For example, numerical modelling suggests Shanghai increases the 2 m air temperature of downwind Kunshan (10 km west of Shanghai) by 0.2–0.4 °C in the afternoon and by 0.4–0.6 °C in the evening [14]. It has been suggested UHI effects could possibly be reduced by 1.25 °C (25% reduction) if upwind urban areas were replaced with natural vegetation [15]. Given the increasing frequency of urban conglomerations, sometimes called urban archipelagos, the impact of cities beyond their boundaries needs to be explored, especially associated with HWs.

Lowry [16] provides a framework to assess the total climate impacts (M) at a station (x) as a function of background climate (C), local landscape impacts (L), and local urbanization impacts (E) for different weather elements (i) for a time period (t):

$$M_{itx} = C_{itx} + L_{itx} + E_{itx} \tag{1}$$

Urban impacts are easily detected if C and L do not change for the same t and x—or, if no urban impacts on climate exist at t = 0 when $E_{itd} = 0$. In the latter case, upwind (u) − downwind (d) differences can be determined from

$$M_{itd} - M_{itu} = (C_{itd} - C_{itu}) + (L_{itd} - L_{itu}) + E_{itd} \tag{2}$$

Here, this framework is used to assess the impact of urbanization on downwind cities.

As urban expansion may bring some negative effects, various mitigation measures have been explored, such as green roofs (GRs). Sharma et al. [17] suggest that daytime roof temperatures can be reduced by 1–3 °C in the Chicago metropolitan area, and the amount will vary linearly with increasing green roof fractions based on urbanized weather research and forecasting (uWRF) simulations. The urban heat stress could potentially be almost completely offset if green roofs were irrigated in New York City and Phoenix during heat wave periods [18]. Green roofs modify wind conditions, with the siting of GRs playing an important role under windy conditions [19].

Here, we explore the impact of urban expansion on cities during HWs, using the megacity Hangzhou (Figure 1) and its effect on a downwind city Haining (Figure 1) through numerical simulations. The specific objectives are to (1) analyze the effect of the upwind megacity size on the UHI size during HW conditions, (2) assess the evolution of spatial and temporal changes of temperature and humidity from horizontal advection from the megacity (Hangzhou) on the smaller city (Haining), and (3) evaluate the downwind effectiveness of a mitigation option (GRs) implemented in the upwind megacity.

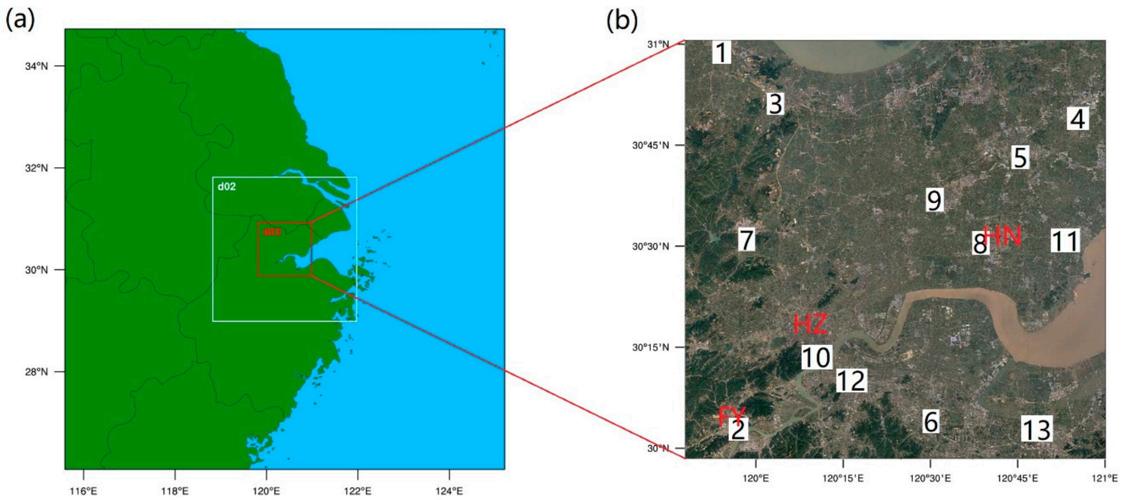

Figure 1. Study area (**a**) model domains d01, d02, and d03, with 9, 3, and 1 km horizontal resolution, respectively; and (**b**) Hangzhou (HZ), Haining (HN), Fuyang (FY), and 13 China Meteorological Administration (CMA) observation sites (numbers). (Source of base maps: Google Timelapse [20]).

2. Methodology

2.1. Study Area

Hangzhou (30°16′ N, 120° 12′ E), the capital of Zhejiang Province, is located 180 km southwest of Shanghai in the Yangtze River Delta (Figure 1b). The city covers 4876 km^2 of the 16,596 km^2 total administrative area. In 2015, the population was 9 million (80% classified as urban) [21]. The city experiences a subtropical climate (mean annual temperature = 16.2 °C), with daily averages ranging from 3.8 °C (winter) to 28.6 °C (summer) [22]. Historically, Hangzhou was renowned for its pleasant weather [23], but in recent years there have been very hot summers (e.g., 42.8 °C on 10 August 2013 [21]). The average annual rainfall (2000–2015) is about 1490 mm [21].

To analyze the impacts of upwind urban expansion on regional climate, two small cities near Hangzhou are studied (Figure 1b): (1) Haining (50 km northeast of Hangzhou, downwind) and (2) Fuyang (30 km southwest of Hangzhou, upwind). These two cities have approximately the same size, population, and climate. These us allow to consider upwind and downwind impacts of the climate (Equation 2).

2.2. Heat Wave Characteristics

The HWs are characterized using daily maximum air temperature data [24,25] for the period 1 January 1979 to 31 December 2014, using the Meehl and Tebaldi [26] HW definition selected within ExtremeFinder/Urban Multi-scale Environmental Predictor (UMEP) [27]. HWs have become more frequent, especially after 2003, with events almost every year (Figure 2). Given that the 2013 HW had the longest duration (31 days) and was the hottest (40.6 °C), we analyze that period. During this HW, the average daily maximum temperature was 36.8 °C, with seven days >39 °C and three days >40 °C.

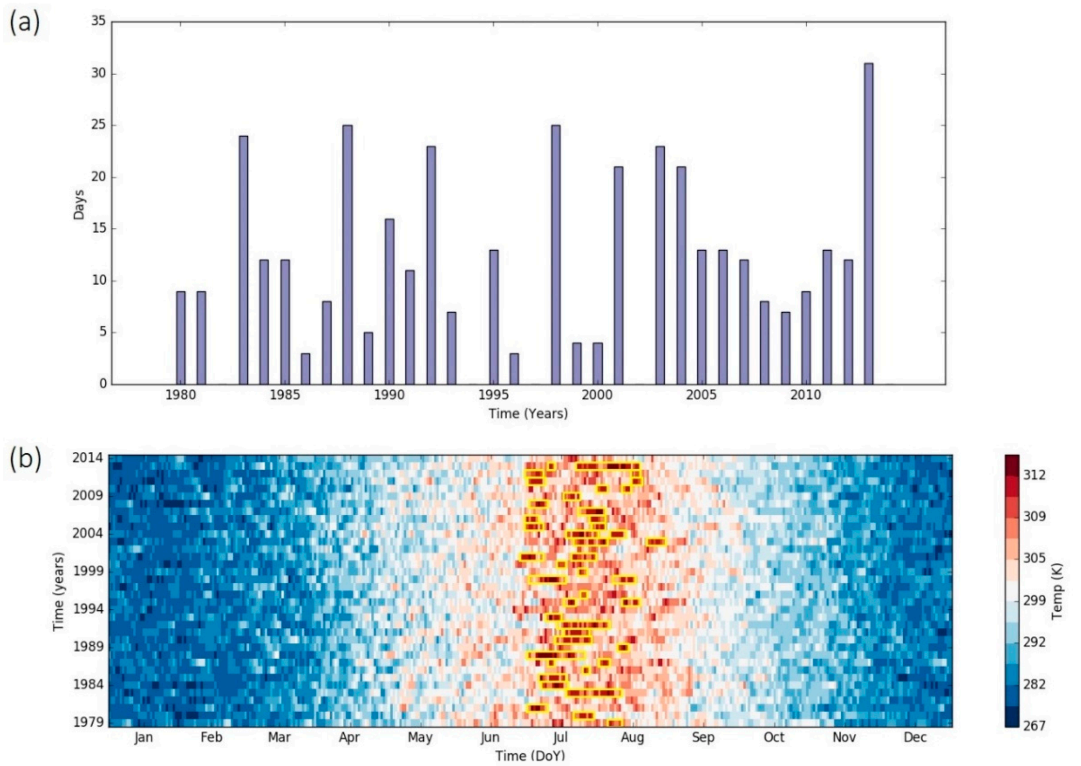

Figure 2. Heat waves in Hangzhou (1 January 1980 to 31 December 2014) by year: (**a**) duration and (**b**) days (yellow boxes) and their maximum temperature. See Section 2.2 for methods.

2.3. Simulation Configuration

To investigate this, we used the weather research and forecasting model (WRF) [28], coupled with the single layer urban canopy model (UCM). The single-layer UCM (urban canopy model) [29,30] has been extensively evaluated in urban areas, both offline (e.g., energy balance fluxes [31,32]) and online (e.g., 2 m temperature [15] and fluxes [33]).

To explore the impact of changing the roof materials, the Princeton roof model (PROM) [34] within the Princeton urban canopy model (PUCM) was used, as it allows the roof facet materials [2,35–38] to be changed, while otherwise retaining the same physics as the UCM.

The Hangzhou area is modeled using three nested domains (horizontal grid resolutions of 9, 3, and 1 km; Figure 1) and IGBP (International Geosphere-Biosphere Programme) -Modified, MODIS (moderate resolution imaging spectroradiometer) 20-category land use [39]. The outer domain (d01) covers most of eastern China; d02 includes Shanghai and most of Zhejiang, as well as a small part of Jiangsu and Anhui provinces; and d03 covers Hangzhou, most of Shaoxing, Jiaxing, and Huzhou, as well as part of the Zhoushan region. The analysis presented is for d03. One-way nesting with 85 sigma levels vertically below the upper boundary of 100 hPa are used in the simulations. The model is run only for part of the HW period (00:00 UTC 30 June 2013 to 00:00 UTC 7 July 2013), with the first 40 hours being model spin-up prior to the analysis periods beginning at 00:00 LST 2 July 2013.

NCEP (National Centers for Environmental Prediction) FNL (final) operational global analysis data [40] are used for both the initial and the boundary conditions. The model physical parameterization schemes chosen are (1) two-dimensional (2D) Smagorinsky [41], the Smagorinsky [42] scheme for horizontal diffusion; (2) the Mellor–Yamada–Janjić planetary boundary layer (PBL) scheme [43,44]; (3) the unified Noah land-surface model; and (4) the rapid radiative transfer model [45] for longwave radiation and the Dudhia [46] scheme for shortwave radiation. The cumulus parameterization option is off for all domains, as even the largest grid size (9 km) is less than 10 km [47], and there was no precipitation during the simulation period. Only the roof parameters differ between the UCM and PUCM/PROM simulations (Table 1, [2,29]). The latter allows GRs to be simulated.

Table 1. Parameters used in the simulations [38]. *Green roofs (GRs) are 0.1 m taller.

Parameter	UCM (Urban Canopy Model) (Roof)	PCUM (Princeton Urban Canopy Model) (Green Roof)
Roof Heat Capacity [J m^{-3} K^{-1}]	1.0×10^6	1.9×10^6
Thermal Conductivity [J m^{-1} s^{-1} K^{-1}]	0.67	1.00
Surface Albedo	0.20	0.30
Surface Emissivity	0.90	0.95
Depth of Green Roof * [m]		0.1
Fraction of Roofs that are GR		0.5
Anthropogenic Heat [W m^{-2}]	50 (Maximum)	
Diurnal Profile of Anthropogenic Heat	0.16, 0.13, 0.08, 0.07, 0.08, 0.26, 0.67, 0.99, 0.89, 0.79, 0.74, 0.73, 0.75, 0.76, 0.82, 0.90, 1.00, 0.95, 0.68, 0.61, 0.53, 0.35, 0.21, 0.18	

2.4. Numerical Experimental Design

To assess the impact of expansion of the Hangzhou urban area, four different urban extents (UE) are simulated (Figure 3):

1. $UE_{1.0}$: current urban extent (IGBP-Modified MODIS 20-category data [48]);
2. $UE_{1.5}$: a 1 km outward expansion in both the east–west and north–south directions (water body grids remain unchanged), creating an urban area 152.3% of the present-day extent;
3. $UE_{0.5}$: an urban contraction in both directions, to become 57% of the current extent (area is replaced with crops, water areas unchanged);
4. $UE_{0.0}$: all urban grids (Figure 3) changed to crops.

The expansion process is similar to the actual urbanization of Hangzhou [24], and some general conclusions are obtained under this type of urban growth.

To consider the potential of green roofs to mitigate HW effects, the GR are assumed to have an initial soil moisture of 0.3 m^3 m^{-3} (~50% saturation, i.e., very well irrigated), to ensure that evaporation [48] is considered over three areal extents:

1. GR_{d03}: GRs added to all roofs in the d03 urban grids (Figure 4a)
2. GR_{HZ}: GRs added to all roofs in the Hangzhou urban grids only (Figure 4b)
3. GR_{NO}: no GRs (Figure 4c).

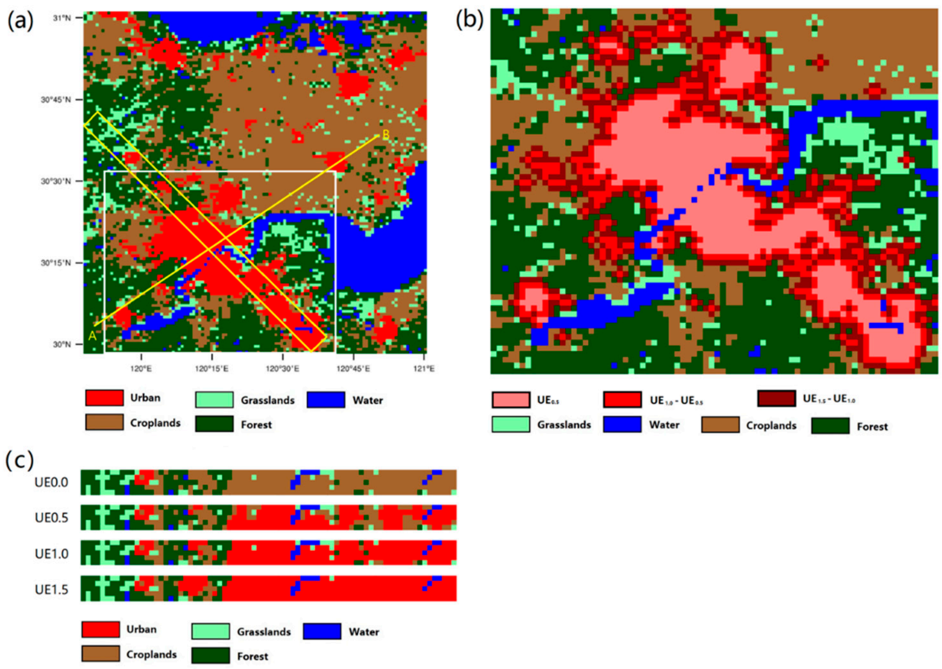

Figure 3. IGBP-modified MODIS 20-category land use [48] in (**a**) d03 (Figure 1a) with the location of the area modified in the four scenarios (Section 2.5) (white rectangle, detail in (**b**)); cross-section analyzed (yellow rectangle, detail in (**c**) of modified urban extent); and the vertical cross-section (yellow line AB, see Figures 9 and 10); (**b**) modified (Section 2.5) land use; and (**c**) detail of area analyzed for the four scenarios (in Figures 6 and 11).

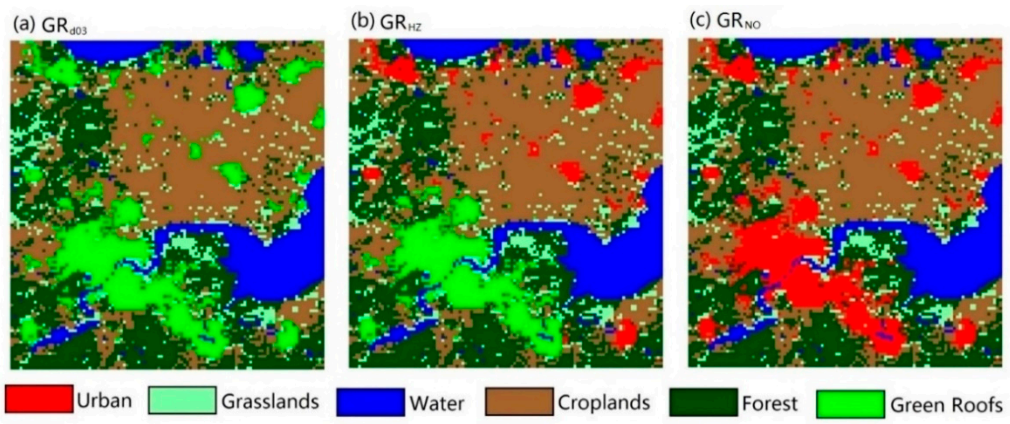

Figure 4. Land use with GRs implemented in (**a**) GR_{d03} all d03 urban grid roofs, (**b**) GR_{HZ} roofs in Hangzhou urban grids, (**c**) GR_{NO} no green roofs.

2.5. *Evaluation of Model Performance*

Near-surface observations at 13 China Meteorological Administration (CMA) meteorological stations in d03 (Figure 1b) over 48 h (00:00 4 July 2013 to 00:00 6 July 2013 UTC) during this HW were used to assess the performance of WRF–UCM (or WRF–PUCM/PROM with no GR). The correlation coefficients of 2 m air temperatures are mostly greater than 0.9 (Figure 5a), but the 2 m temperature is underestimated (mean bias error (MBE) = −1.03 °C). This is consistent with previous findings [49,50]. This leads to overestimation of 2 m relative humidity (MBE = 14.54%), but generally reasonable correlation coefficients (>0.8). The 10-m wind speed correlation coefficients are mostly between 0.4 to 0.8. The wind direction hit rate (HR, [51]) for within 30° of observed values is 45%. Unfortunately, WRF-PROM with larger GR extents cannot be evaluated, as there are currently insufficient GRs in the area to evaluate with meteorological observation sites available. Prior to this, WRF-PUCM/PROM evaluations at both Tsinghua University in Beijing, China and Princeton University in New Jersey, United States, found that PROM is able to capture the diurnal cycle of roof temperatures and the soil moisture dynamics of green roofs with high accuracy. [38].

Of interest are the sites in Hangzhou (#10) and in the downwind city Haining (#8). For both there is very good performance (correlation coefficients are >0.95 and >0.9, respectively) for both 2 m air temperature and 2 m relative humidity, with consistent performance across the diurnal cycle as well.

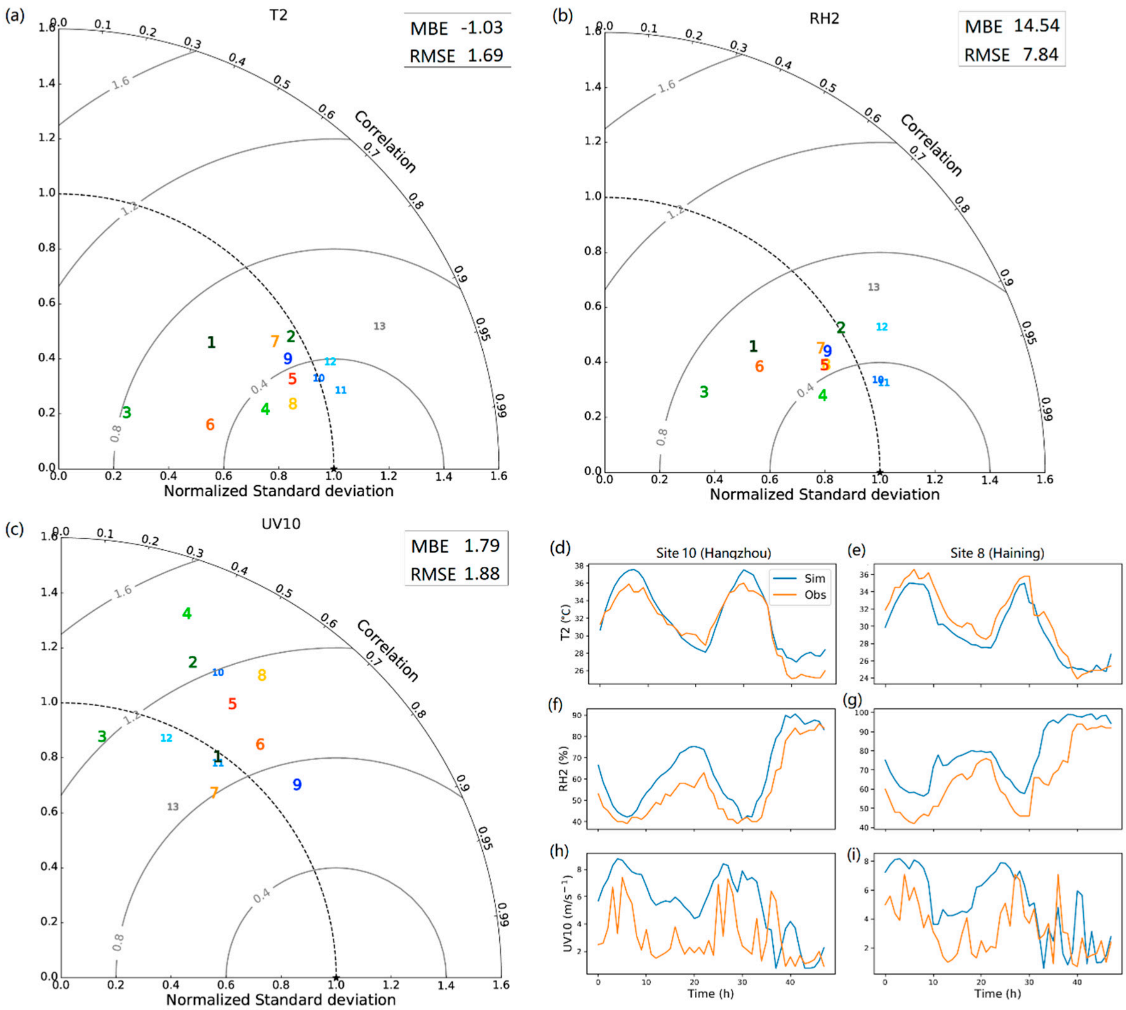

Figure 5. Weather research and forecasting (WRF)–urban canopy model (UCM) performance (00:00 4 July 2013 to 00:00 6 July 2013 UTC), evaluated using measurements at 13 CMA sites in Zhejiang Province (Figure 1b) for (**a**) 2 m air temperature (°C), (**b**) 2 m relative humidity (%), (**c**) 10 m wind speed (m s^{-1}), as well as time series of (**d**,**e**) 2 m air temperature (°C), (**f**,**g**) 2 m relative humidity (%), and (**h**,**i**) 10 m wind speed (m s^{-1}) for sites (**d**,**f**,**h**) #10 (Hangzhou) and (**e**,**g**,**i**) #8 (Haining). (**a**–**c**) Taylor [52] plots are for hourly data with correlation coefficients (polar axis), with normalized standard deviation (horizontal axis) and normalized root mean square error (RMSE) (internal circular axes). The overall, cross-site, mean bias error (MBE) and RMSE are also indicated.

3. Impacts of the Upwind Megacity Size

To examine the impacts of increasing city size during an HW period (Figure 6), the variables analyzed are the surface energy balance fluxes (storage heat flux, turbulent sensible, and latent heat fluxes) and the resulting impacts from the surface energy balance flux changes (i.e., surface temperature, 2 m air temperature, 2 m specific humidity, and 10 m wind speed). The variables are analyzed spatially, using transects that are perpendicular to the predominantly southwesterly wind direction (Figure 3c) (background wind, Appendix A). The spatial means (5 km) are determined from the 1 km grids for 3 h time periods. This gives eight time series for each variable investigated.

With the expansion of the urban area ($UE_{1.5}$–$UE_{1.0}$ difference), the storage heat flux has an enhanced diurnal cycle, with larger positive values during the day and larger negative values at night. As expected, there are larger storage heat fluxes in the urban area. Similarly, the turbulent sensible heat fluxes increase and latent heat fluxes decrease with the reduction in vegetation and therefore soil moisture in the urban areas.

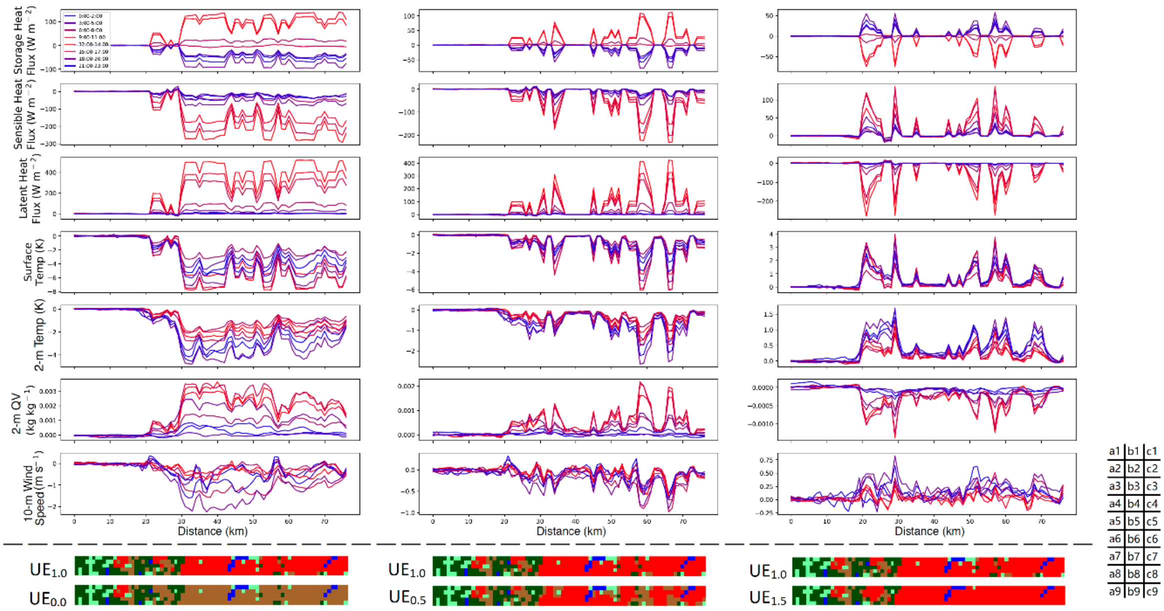

Figure 6. Average difference in (**1**) storage heat flux; (**2**) turbulent sensible heat flux at the surface; (**3**) turbulent latent heat flux at the surface; (**4**) surface temperature; (**5**) 2 m air temperature; (**6**) 2 m specific humidity; (**7**) 10 m wind speed, with changes in urban extent $UE_{1.0}$ and (**a**) $UE_{0.0}$, (**b**) $UE_{0.5}$, (**c**) $UE_{1.5}$ scenarios (Section 2.5) along cross-sections (location: Figure 3a) for eight 3 h periods (averaged 2 to 5 July 2013 local standard time LST); and land use of the cross-section for (**8**) before case and (**9**) after case (see also Figure 3c).

Daytime surface temperature differences are warmer, but 2 m air temperature decreases, with even larger changes at night, as urban areas absorb more heat during the day and release it at night. This results in an increased 2 m nocturnal air temperature. Urban development also influences humidity, with a more evident "dry island" as the modeled city grows. A decrease of 3.5 g kg^{-1} in the daytime of the 2 m specific humidity is simulated between $UE_{0.0}$ and $UE_{1.0}$ (Figure 6a). As the 2 m temperature increases, the specific humidity is reduced, especially during daytime when the temperature is relatively high. Wind speed is also affected by urbanization. The urban expansion is associated with larger nocturnal wind speeds. This is consistent with Kang and Lenschow's [53] findings (WRF–LES (large eddy simulation) simulations) of surface heterogeneity causing larger winds perpendicular to the mesoscale wind direction. Similarly, in the Hangzhou simulation, high pressure influencing the region creates a continuous background wind that is enhanced by the urban-induced thermal difference. The strongest wind speed difference occurs at night, associated with the greater thermal heterogeneity.

The influence of land use changes is consistent between variables along the cross-section (Figure 6a), with the unchanged water bodies evident. Comparing Figure 6a,b, the trend for the three land use scenarios is similar through the day. However, the location of the changes varies, from all of Hangzhou (Figure 6a: urban expansion, $UE_{1.0} - UE_{0.0}$) to mainly on the edge of Hangzhou (Figure 6b: $UE_{1.0} - UE_{0.5}$). This is as expected with the land use changes simulated. Note that the variables in the center of Hangzhou are almost unaffected (Figure 6b,c), suggesting that the impact of urban expansion on surrounding cities is not obvious in the direction perpendicular to the background wind.

Potential temperatures within the planetary boundary layer (PBL) change between the land use scenarios (Figure 7), with larger differences during the day than at night. The maximum near surface difference (0.2 °C) is at 13:00. The changes in potential temperatures are consistent with PBL height changes, indicating that urban expansion modifies the thermal regime throughout the PBL. A deeper PBL can result in enhanced heating because of entrainment. A decrease of 0.1 °C in potential temperature is simulated at 23:00 near the top of the PBL (~200 m agl WRF determined), and is attributed to the temperature inversion in the entrainment zone.

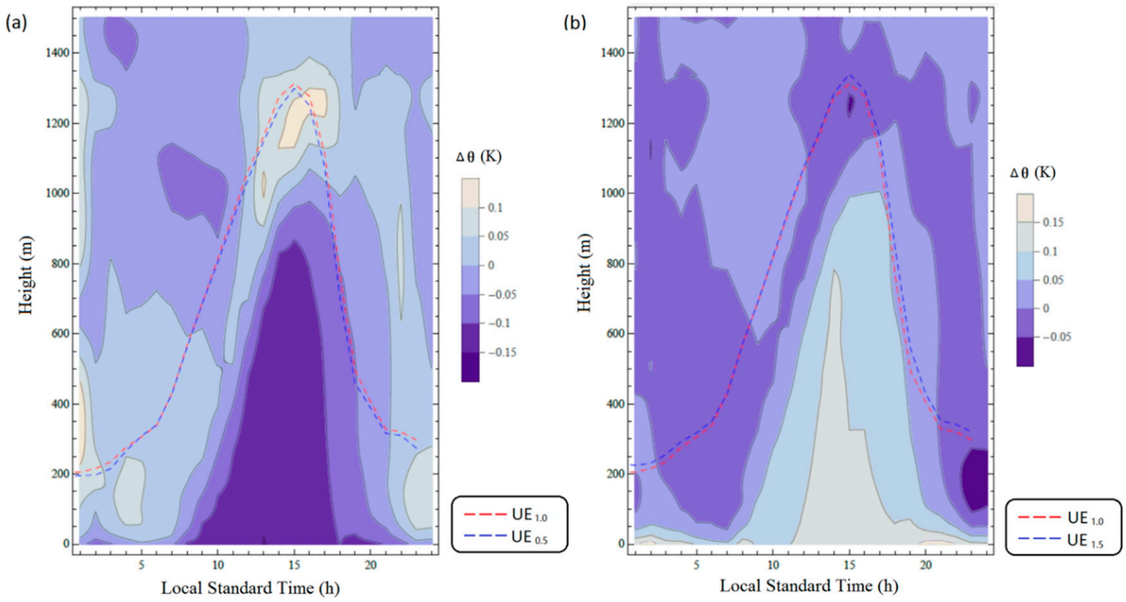

Figure 7. Mean (2–5 July 2013 LST) vertical potential temperature difference (Δθ) between scenarios: (**a**) $UE_{0.5}$ and $UE_{1.0}$, and (**b**) $UE_{1.5}$ and $UE_{1.0}$ in Hangzhou. Height of urban boundary layer, as diagnosed by Mellor and Yamada [44] and Janjić [45] planetary boundary layer (PBL) scheme.

4. Impacts on the Downwind Regions

The simulations show that urbanization of Hangzhou has a negative impact (i.e., warming), not only on Hangzhou but also the surrounding area, especially downwind of Haining (Figure 1b). The impact on Haining varies between $UE_{0.5}$, $UE_{1.0}$ and $UE_{1.5}$ (Figure 8).

Following Lowry's [16] methodology (Equations 1 and 2), analyzing changes in Fuyang (a small city upwind of Hangzhou, Figure 1b) is useful to rule out other influences. In Fuyang, the urban expansion in Hangzhou results in negligible changes to storage, as well as turbulent-sensible and latent heat fluxes. However, differences in temperature, humidity, and wind speed from urban expansion are much more evident in Haining (downwind of Hanghzou) than in Fuyang, highlighting the impact of urbanization downwind. The 2 m temperature changes were mainly at night, while specific humidity changed mainly during the day. This is consistent with the temporal pattern (Figure 6), supporting the explanation that the cause is the expansion of Hangzhou.

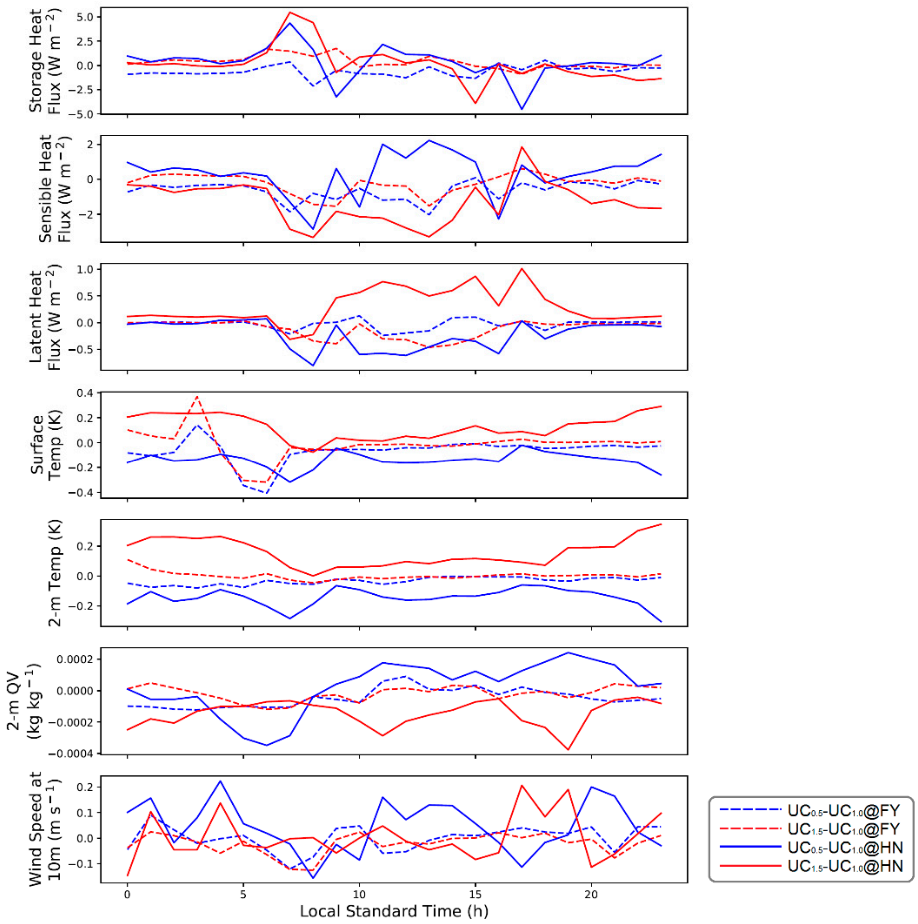

Figure 8. Temporal (2–5 July 2013 LST) and spatially-averaged differences of diurnal (**a**) storage heat flux, (**b**) surface turbulent sensible heat flux, (**c**) surface turbulent latent heat flux, (**d**) surface temperature, (**e**) 2 m air temperature, (**f**) 2 m specific humidity, and (**g**) 10 m wind speed in Fuyang (FY, dashed) and Haining (HN, solid; see Figure 1b) for differences between scenarios (Section 2.5): $UE_{0.5} - UE_{1.0}$ (blue) and $UE_{1.5} - UE_{1.0}$ (red).

The vertical cross-section (Figure 2, transect AB) of the difference in 2 m air temperatures between the $UE_{0.5}$ and $UE_{1.0}$ scenarios has a clear nocturnal increase of more than 1 °C in the rural region that has become urban (Figure 9). This impact extends into areas where land use has not changed, nearly 30 km upwind and more than 50 km downwind. The maximum temperature difference downwind (0.36 °C) is almost twice of the difference at an equivalent distance upwind (0.19 °C). The spatial extent of the influence upwind and the size of the temperature difference are both larger at night, which is consistent with the diurnal cycle of air temperature change in Hangzhou. However, the extent of influence downwind is large during the day because of stronger winds (i.e., a secondary impact in the downwind regions). The result, between $UE_{1.0}$ and $UE_{1.5}$, also gets an approximate conclusion.

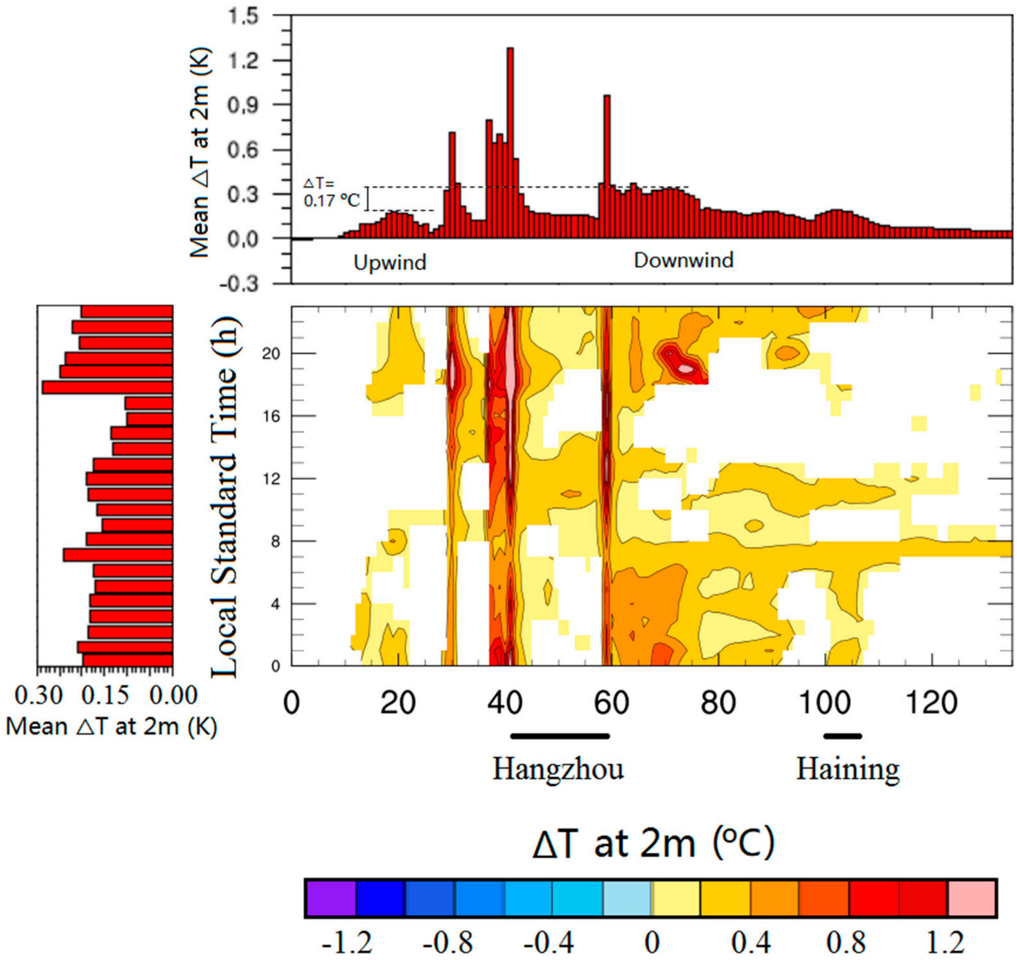

Figure 9. Mean (2–5 July 2013 LST) diurnal 2 m air temperature difference (in K) between the $UE_{0.5}$ and $UE_{1.0}$ scenarios (Section 2.5) along line AB (see Figure 3a). The values between −0.1 °C and 0.1 °C are masked.

Turbulent sensible heat flux increases by more than 160 W m^{-2} in the daytime in rural regions that are urbanized (Figure 10). This is consistent with the changes in air temperature (Figure 9). However, the sensible heat flux difference in the downwind urban area, where the 2 m air temperature increases, is close to zero, suggesting that it is not driving the 2 m temperature change downwind. Similarly, small changes occur in the storage and latent heat fluxes (Figure 8). This supports that advection is the critical influence with regard to relative humidity changing with the increasing temperature.

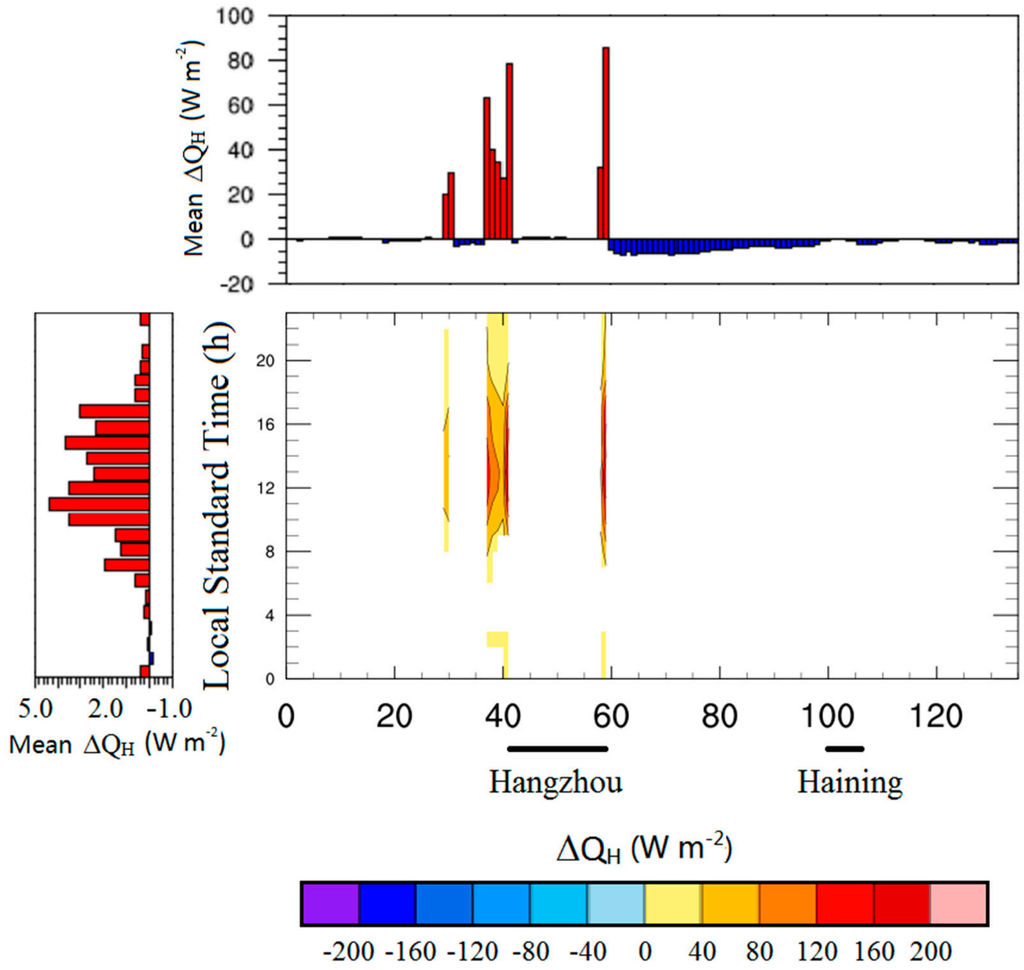

Figure 10. The same as Figure 9, but with surface turbulent sensible heat flux (W m^{-2}). The values between -5 W m^{-2} to 5 W m^{-2} are masked.

5. Can these Urban Expansion Impacts Be Mitigated with Green Roofs?

Green roofs (GRs) are one potential strategy to mitigate temperature effects in and downwind of a city. Analysis of the difference between simulations when all the urban roofs in d03 are assumed to be green (GR_{d03}) and when none are green (GR_{NO}) (Section 2.5) shows a reduction in sensible heat flux (maximum 55 W m^{-2}) and an increase in latent heat flux (maximum 85 W m^{-2}). For both fluxes, the largest difference occurs in the daytime. Associated with these changes in turbulent fluxes are small reductions in surface temperature during the day and night of 1.5 °C and 0.5 °C, respectively. This is consistent with the sensible heat flux changes. The effect of GRs is to reduce the amplitude of the diurnal cycle of the storage heat flux. This is attributed to an increase in heat storage capacity in urban areas by green roofs (especially while wet). Thus, in these simulations GRs do mitigate UHI effects, and could reduce surface temperature in cities during the daytime (if sufficient water was available). The size of the changes is potentially large enough to have an impact—for example, Anderson [1] suggests that a 0.5 °C decrease in 2 m air temperature (Figure 11e) decreased mortality risk by 2.25% during a HW in the United States. Other impacts simulated include an increase of 0.6 g kg^{-1}, 2 m-specific humidity, as well as a decrease of 0.4 m s^{-1}, 10 m wind speed during the daytime. The reduction of wind speed may improve thermal comfort with less advected heat into the urban area. However, the higher humidity and lower wind speed may not be more pleasant.

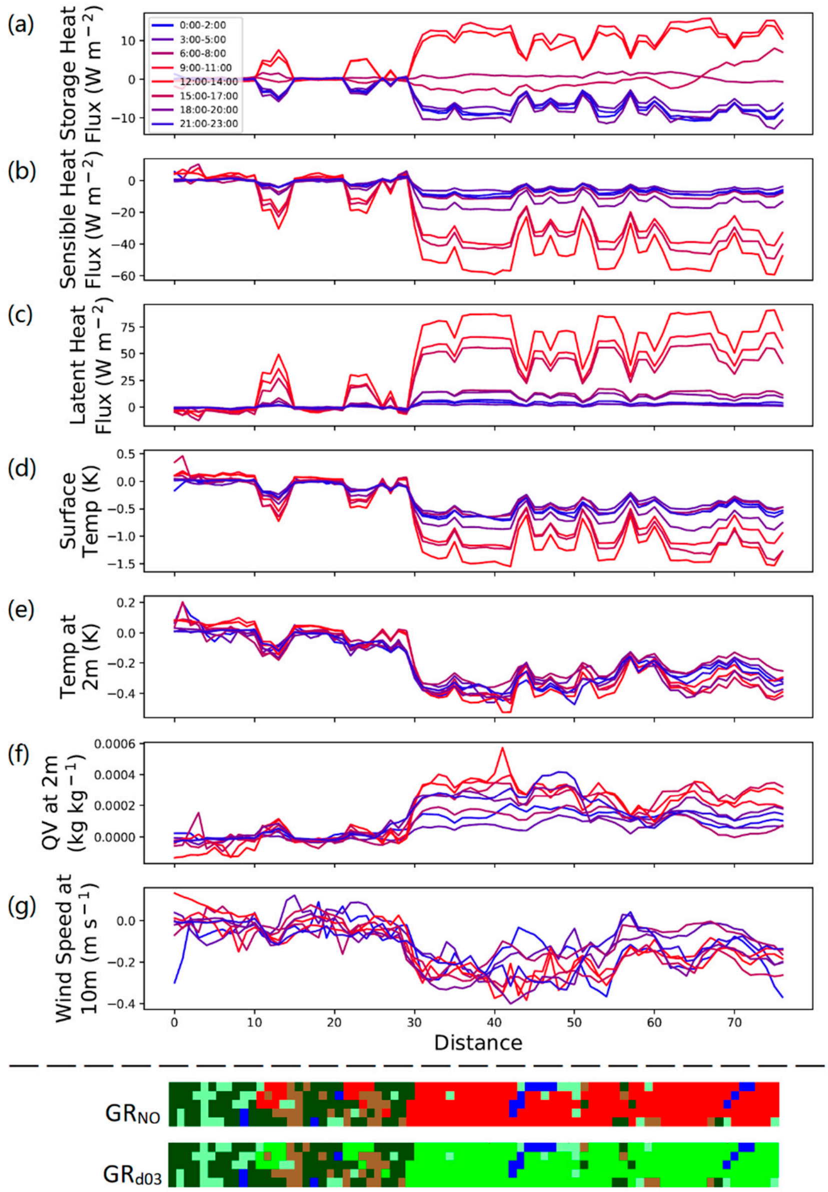

Figure 11. The same as Figure 6, but between GR_{d03} (green roofs added to all roofs in the d03 urban grids) and GR_{NO} (no green roofs) scenarios (Section 2.5).

The results also indicate that GRs modify the potential temperature and PBL height (Figure 12). The GRs in upwind cities (GR_{HZ} scenario, Figure 12a) result in a reduction of potential temperature (0.2 °C) and a decrease in the daytime PBL height (~50 m). Effects such as this are important to explore in the context of air quality. The GRs could alleviate the thermal effects of urban expansion on the downwind cities. The maximum potential temperature difference in Haining was 0.25 °C (GR_{HZ} and GR_{NO} scenarios, see Figure 12b), which is greater than the change in Hangzhou itself. As the timing of maximum differences vary (Hangzhou 13:00, Haining 17:00), this suggests the mitigation in Haining is due to advection. The GRs decrease the wind speed in downwind cities.

The green roofs greatly reduce the air temperature of Hangzhou and the downwind city Haining, and can be used to mitigate thermal effects of regional urban expansion. This result is expected to have important implications for planning scenarios and decisions regarding where mitigation strategies have maximum effects, both locally and regionally (downwind).

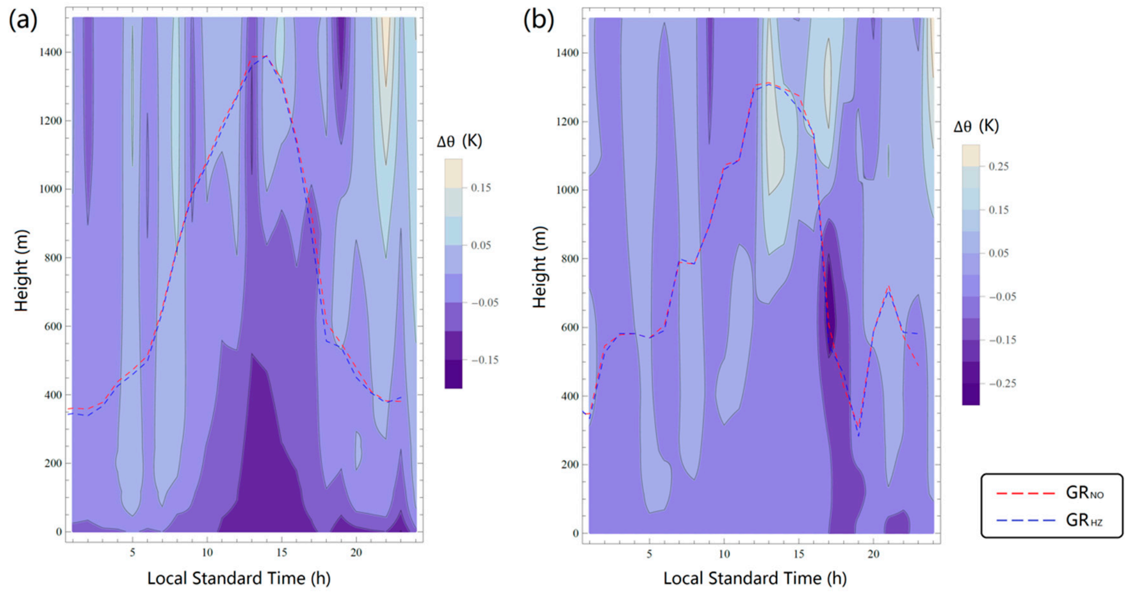

Figure 12. The same as Figure 7, but for GR_{NO} and GR_{HZ} (all green roofs in Hangzhou urban grids) scenarios, in (**a**) Hangzhou and (**b**) Haining (see Figure 1b).

6. Concluding Remarks

This study investigates the impacts of upwind urbanization on the UHI effects of downwind cities, by conducting numerical simulations in the Yangtze River Delta Region for the heat wave conditions of 2013. Four scenarios of Hangzhou's extent are modelled. From analysis of these results, the following conclusions are drawn:

- Without the urban surface of Hangzhou, the 2 m temperature is 5 °C lower at night, and the 2 m specific humidity is 3.5 g kg^{-1} higher during the daytime, compared to the current urban extent ($UE_{1.0}$).
- With increasing urban expansion, an increase of nighttime 2 m air temperature of 2.7 °C for $UE_{0.5}$ to $UE_{1.0}$, and 1.7 °C for $UE_{1.0}$ to $UE_{1.5}$, as well as a 2.1 g kg^{-1} and 1.4 g kg^{-1} decrease, respectively, of daytime 2 m specific humidity are predicted.
- Greater heat flux heterogeneity caused by urban areas leads to an increase of 1.0 and 0.8 m s^{-1} for 10 m wind speed in Hangzhou.
- Comparison of the conditions for a small city upwind (Fuyang) and downwind (Haining) of the megacity (Hangzhou) indicates large impacts from upwind urban expansion on regional climate.
- Given the predominant southwesterly winds, the urbanization in Hangzhou increases 2 m air temperature in Haining by about 0.3 °C between $UE_{0.5}$ and $UE_{1.0}$, and 0.4 °C between $UE_{1.0}$ and $UE_{1.5}$, while the increases are about 0.05 °C and 0.1 °C, respectively, for Fuyang.
- The strongest and widest warming effect appears at 0700 LST, and the weakest effect occurs in the afternoon. Similar results are predicted for 2 m specific humidity and 10 m wind speed.

The driving heat flux changes in Haining are less than 5 W m^{-2}, but vary by hundreds of W m^{-2} in Hangzhou. This suggests that it is advection that give rise to the atmospheric changes in Haining.

One mitigation strategy (green roofs) is examined in the upwind megacity. From the simulations, the following conclusions are drawn:

- Green roof coverage of 50% in the d03 area could reduce the daytime 2 m air temperature in Hangzhou by 0.5 °C, and increase the 2 m specific humidity by 0.6 g kg^{-1}. Such changes effectively alleviate the UHI effect and the "dry island" effect within Hangzhou.
- Green roofs in Hangzhou can relieve the thermal stress in the downwind city Haining by decreasing the potential temperature by 0.25 °C.

- The strongest mitigation effects appear at 1300 LST in Hangzhou and 1600 LST in Haining.

  Overall it is concluded:

- City location is important within an urban cluster as a modifier of urban microclimate.
- Green roofs may have the potential to mitigate some of the urban effects in a chain of cities.
- There are differential effects in cities and linked impacts in proximal cities.

Author Contributions: Conceptualization, G.N. and S.G.; methodology, B.H. and S.G.; evaluation, B.H.; formal analysis, B.H..; investigation, B.H.; resources, S.G.; writing—original draft preparation, B.H.; writing—review and editing, G.N. and S.G.; visualization, B.H. and S.G.; supervision, G.N. and S.G.

Funding: National Key Research and Development (R&D) Plan of China, grant number 2018YFA0606002 (G.N.), Newton Fund/Met Office CSSP-China (S.G.). The British Council supported B.H.'s visit to University of Reading.

Acknowledgments: Data from this paper are available through request to the author via b-huang14@mails.tsinghua.edu.cn. Meteorological initial and lateral boundary condition data sets are available at the NCEP (National Centers for Environmental Prediction) FNL (Final) Operational Global Analysis data (https://rda.ucar.edu/datasets/ds083.2/#!access). Computation was supported by the National Supercomputer Center in Guangzhou (NSCC-GZ).

Conflicts of Interest: The authors declare no conflict of interest.

Appendix A

The prevailing wind for the whole HW period was from the southwest. The wind speed at 10 m reached 8 m s^{-1} during the daytime (Figure A1). Thus, Haining was always downwind of Hangzhou in the study period.

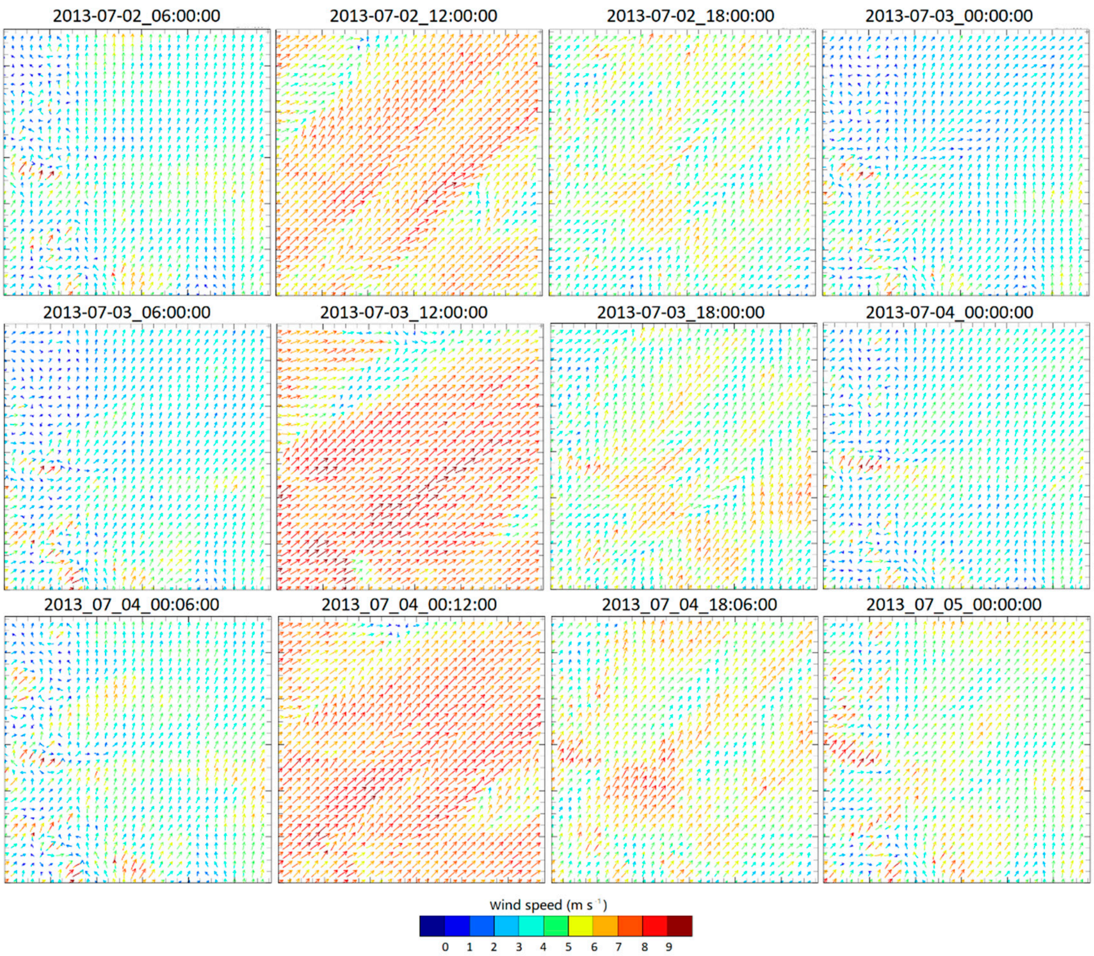

Figure A1. Simulated d03 (Figure 1) wind vectors every six hours (2–5 July 2013 LST).

References

1. Anderson, G.B.; Bell, M.L. Heat waves in the United States: Mortality risk during heat waves and effect modification by heat wave characteristics in 43 U.S. communities. *Environ. Health Perspect.* **2011**, *119*, 210–218. [CrossRef] [PubMed]
2. Li, D.; Bou-Zeid, E.; Oppenheimer, M. The effectiveness of cool and green roofs as urban heat island mitigation strategies. *Environ. Res. Lett.* **2014**, *9*, 055002. [CrossRef]
3. Kalkstein, L.S. Direct impacts in cities. *Lancet* **1993**, *342*, 1397–1399. [CrossRef]
4. Weisskopf, M.G.; Anderson, H.A.; Foldy, S.; Hanrahan, L.P.; Blair, K.; Török, T.J.; Rumm, P.D. Heat wave morbidity and mortality, Milwaukee, Wis, 1999 vs 1995: An improved response? *Am. J. Public Health* **2002**, *92*, 830–833. [CrossRef] [PubMed]
5. Arnfield, A.J. Two decades of urban climate research: A review of turbulence, exchanges of energy and water, and the urban heat island. *Int. J. Climatol.* **2003**, *23*, 1–26. [CrossRef]
6. Pielke Sr, R.A.; Adegoke, J.; BeltraáN-Przekurat, A.; Hiemstra, C.A.; Lin, J.; Nair, U.S.; Nobis, T.E. An overview of regional land-use and land-cover impacts on rainfall. *Tellus B Chem. Phys. Meteorol.* **2007**, *59*, 587–601. [CrossRef]
7. Li, D.; Bou-Zeid, E. Synergistic interactions between urban heat islands and heat waves: The impact in cities is larger than the sum of its parts. *J. Appl. Meteorol. Climatol.* **2013**, *52*, 2051–2064. [CrossRef]
8. Ramamurthy, P.; Li, D.; Bou-Zeid, E. High-resolution simulation of heatwave events in New York City. *Theor. Appl. Climatol.* **2017**, *128*, 89–102. [CrossRef]
9. Li, D.; Sun, T.; Liu, M.; Yang, L.; Wang, L.; Gao, Z. Contrasting responses of urban and rural surface energy budgets to heat waves explain synergies between urban heat islands and heat waves. *Environ. Res. Lett.* **2015**, *10*, 054009. [CrossRef]
10. Li, D.; Sun, T.; Liu, M.; Wang, L.; Gao, Z. Changes in wind speed under heat waves enhance urban heat Islands in the Beijing metropolitan area. *J. Appl. Meteorol. Climatol.* **2016**, *55*, 2369–2375. [CrossRef]
11. Sun, T.; Kotthaus, S.; Li, D.; Ward, H.C.; Gao, Z.; Ni, G.-H.; Grimmond, C.S.B. Attribution and mitigation of heat wave-induced urban heat storage change. *Environ. Res. Lett.* **2017**, *12*, 114007. [CrossRef]
12. Oke, T.R. The energetic basis of the urban heat island. *Q. J. R. Meteorol. Soc.* **1982**, *108*, 1–24. [CrossRef]
13. Shepherd, J.M. A review of current investigations of urban-induced rainfall and recommendations for the future. *Earth Interact.* **2005**, *9*, 1–27. [CrossRef]
14. Kang, H.-Q.; Zhu, B.; Zhu, T.; Sun, J.-L.; Ou, J.-J. Impact of megacity Shanghai on the urban heat-island effects over the downstream city Kunshan. *Bound. Layer Meteorol.* **2014**, *152*, 411–426. [CrossRef]
15. Zhang, D.-L.; Shou, Y.-X.; Dickerson, R.R.; Chen, F. Impact of upstream urbanization on the urban heat island effects along the Washington–Baltimore corridor. *J. Appl. Meteorol. Climatol.* **2011**, *50*, 2012–2029. [CrossRef]
16. Lowry, W.P. Empirical estimation of urban effects on climate: A problem analysis. *J. Appl. Meteorol.* **1977**, *16*, 129–135. [CrossRef]
17. Sharma, A.; Conry, P.; Fernando, H.; Hamlet, A.F.; Hellmann, J.; Chen, F. Green and cool roofs to mitigate urban heat island effects in the Chicago metropolitan area: Evaluation with a regional climate model. *Environ. Res. Lett.* **2016**, *11*, 064004. [CrossRef]
18. Tewari, M.; Yang, J.; Kusaka, H.; Palou, F.S.; Watson, C.; Treinish, L. Interaction of urban heat islands and heat waves under current and future climate conditions and their mitigation using green and cool roofs in New York City and Phoenix, Arizona. *Environ. Res. Lett.* **2018**, *14*, 034002. [CrossRef]
19. Yang, J.; Bou-Zeid, E. Scale dependence of the benefits and efficiency of green and cool roofs. *Landsc. Urban Plan.* **2019**, *185*, 127–140. [CrossRef]
20. Google Timelapse. Available online: https://earthengine.google.com/timelapse (accessed on 23 May 2019).
21. Hangzhou Statistical Bureau. Available online: http://www.hangzhou.gov.cn/col/col1224749/index.html (accessed on 23 May 2019).
22. Deng, J.; Li, J.; Yu, L.; Wang, K. Dynamics of land use landscape pattern in Hangzhou City during its rapid urbanization. *Yingyong Shengtai Xuebao* **2008**, *19*, 9.
23. Chen, K. Warming trend and seasonal variation in Hangzhou from 1961 to 2012. *Chin. Agric. Sci. Bull.* **2013**, *29*, 345–350.

24. Weedon, G.; Gomes, S.; Viterbo, P.; Shuttleworth, W.; Blyth, E.; Österle, H.; Best, M. Creation of the WATCH forcing data and its use to assess global and regional reference crop evaporation over land during the twentieth century. *J. Hydrometeorol.* **2011**, *12*, 823–848. [CrossRef]
25. Weedon, G.P.; Balsamo, G.; Bellouin, N.; Gomes, S.; Best, M.J.; Viterbo, P. The WFDEI meteorological forcing data set: WATCH forcing data methodology applied to ERA-interim reanalysis data. *Water Resour. Res.* **2014**, *50*, 7505–7514. [CrossRef]
26. Meehl, G.A.; Tebaldi, C. More intense, more frequent, and longer lasting heat waves in the 21st century. *Science* **2004**, *305*, 994–997. [CrossRef] [PubMed]
27. Lindberg, F.; Grimmond, C.S.B.; Gabey, A.; Huang, B.; Kent, C.W.; Sun, T.; Theeuwes, N.E.; Järvi, L.; Ward, H.C.; Capel-Timms, I.; et al. Urban multi-scale environmental predictor (UMEP): An integrated tool for city-based climate services. *Environ. Model. Softw.* **2018**, *99*, 70–87. [CrossRef]
28. Skamarock, W.C.; Klemp, J.B. A time-split nonhydrostatic atmospheric model for weather research and forecasting applications. *J. Comput. Phys.* **2008**, *227*, 3465–3485. [CrossRef]
29. Kusaka, H.; Kondo, H.; Kikegawa, Y.; Kimura, F. A simple single-layer urban canopy model for atmospheric models: Comparison with multi-layer and slab models. *Bound. Layer Meteorol.* **2001**, *101*, 329–358. [CrossRef]
30. Kusaka, H.; Kimura, F. Coupling a single-layer urban canopy model with a simple atmospheric model: Impact on urban heat island simulation for an idealized case. *J. Meteorol. Soc. Jpn. Ser. II* **2004**, *82*, 67–80. [CrossRef]
31. Loridan, T.; Grimmond, C.; Grossman-Clarke, S.; Chen, F.; Tewari, M.; Manning, K.; Best, M. Trade-offs and responsiveness of the single-layer urban canopy parametrization in WRF: An offline evaluation using the MOSCEM optimization algorithm and field observations. *Q. J. R. Meteorol. Soc.* **2010**, *136*, 997–1019. [CrossRef]
32. Loridan, T.; Grimmond, C.S.B. Multi-site evaluation of an urban land-surface model: Intra-urban heterogeneity, seasonality and parameter complexity requirements. *Q. J. R. Meteorol. Soc.* **2012**, *138*, 1094–1113. [CrossRef]
33. Loridan, T.; Lindberg, F.; Jorba, O.; Kotthaus, S.; Grossman-Clarke, S.; Grimmond, C. High resolution simulation of surface heat flux variability across central London with urban zones for energy partitioning. *Bound. Layer Meteorol.* **2013**, *147*, 493–523. [CrossRef]
34. Yang, J.; Wang, Z.-H.; Chen, F.; Miao, S.; Tewari, M.; Voogt, J.A.; Myint, S. Enhancing hydrologic modelling in the coupled weather research and forecasting–urban modelling system. *Bound. Layer Meteorol.* **2015**, *155*, 87–109. [CrossRef]
35. Wang, Z.H.; Bou-Zeid, E.; Smith, J.A. A coupled energy transport and hydrological model for urban canopies evaluated using a wireless sensor network. *Q. J. R. Meteorol. Soc.* **2013**, *139*, 1643–1657. [CrossRef]
36. Wang, Z.-H.; Bou-Zeid, E.; Au, S.K.; Smith, J.A. Analyzing the sensitivity of WRF's single-layer urban canopy model to parameter uncertainty using advanced Monte Carlo simulation. *J. Appl. Meteorol. Climatol.* **2011**, *50*, 1795–1814. [CrossRef]
37. Wang, Z.-H.; Bou-Zeid, E.; Smith, J.A. A spatially-analytical scheme for surface temperatures and conductive heat fluxes in urban canopy models. *Bound. Layer Meteorol.* **2011**, *138*, 171–193. [CrossRef]
38. Sun, T.; Bou-Zeid, E.; Wang, Z.-H.; Zerba, E.; Ni, G.-H. Hydrometeorological determinants of green roof performance via a vertically-resolved model for heat and water transport. *Build. Environ.* **2013**, *60*, 211–224. [CrossRef]
39. Sun, T.; Grimmond, C.S.B.; Ni, G.-H. How do green roofs mitigate urban thermal stress under heat waves? *J. Geophys. Res. Atmos.* **2016**, *121*, 5320–5335. [CrossRef]
40. National Centers for Environmental Prediction; National Weather Service; NOAA, U.S.; Department of Commerce. NCEP FNL operational model global tropospheric analyses, continuing from July 1999. 2000. Available online: https://rda.ucar.edu/datasets/ds083.2/ (accessed on 23 May 2019).
41. Smagorinsky, J. General circulation experiments with the primitive equations: I. The basic experiment. *Mon. Weather Rev.* **1963**, *91*, 99–164. [CrossRef]
42. Smagorinsky, J. Some historical remarks on the use of nonlinear viscosities. *Large Eddy Simul. Complex Eng. Geophys. Flows* **1993**, *1*, 69–106.
43. Mellor, G.L.; Yamada, T. Development of a turbulence closure model for geophysical fluid problems. *Rev. Geophys.* **1982**, *20*, 851–875. [CrossRef]

44. Janjić, Z.I. The step-mountain coordinate: Physical package. *Mon. Weather Rev.* **1990**, *118*, 1429–1443. [CrossRef]
45. Mlawer, E.J.; Taubman, S.J.; Brown, P.D.; Iacono, M.J.; Clough, S.A. Radiative transfer for inhomogeneous atmospheres: RRTM, a validated correlated-k model for the longwave. *J. Geophys. Res. Atmos.* **1997**, *102*, 16663–16682. [CrossRef]
46. Dudhia, J. Numerical study of convection observed during the winter monsoon experiment using a mesoscale two-dimensional model. *J. Atmos. Sci.* **1989**, *46*, 3077–3107. [CrossRef]
47. Stensrud, D.J. *Parameterization Schemes: Keys to Understanding Numerical Weather Prediction Models*; Cambridge University Press: Cambridge, UK, 2009.
48. Friedl, M. Modified IGBP MODIS 20-Category Vegetation (Land-Use) Data. 2008. Available online: ftp://ftp.emc.ncep.noaa.gov/mmb/gcp/ldas/noahlsm/README (accessed on 23 May 2019).
49. Giannaros, T.M.; Melas, D.; Daglis, I.A.; Keramitsoglou, I.; Kourtidis, K. Numerical study of the urban heat island over Athens (Greece) with the WRF model. *Atmos. Environ.* **2013**, *73*, 103–111. [CrossRef]
50. Chen, F.; Yang, X.; Zhu, W. WRF simulations of urban heat island under hot-weather synoptic conditions: The case study of Hangzhou City, China. *Atmos. Res.* **2014**, *138*, 364–377. [CrossRef]
51. Schlünzen, K.H.; Katzfey, J.J. Relevance of sub-grid-scale land-use effects for mesoscale models. *Tellus A Dyn. Meteorol. Oceanogr.* **2003**, *55*, 232–246. [CrossRef]
52. Taylor, K.E. Summarizing multiple aspects of model performance in a single diagram. *J. Geophys. Res. Atmos.* **2001**, *106*, 7183–7192. [CrossRef]
53. Kang, S.-L.; Lenschow, D.H. Temporal evolution of low-level winds induced by two-dimensional mesoscale surface heat-flux heterogeneity. *Bound. Layer Meteorol.* **2014**, *151*, 501–529. [CrossRef]